Anna von der Heydt
IMAU
Utrecht University
a.s.vonderheydt@uu.nl

Henk Dijkstra
IMAU
Utrecht University
h.a.dijkstra@uu.nl

El Niño: processes, dynamics and predictability

The El Niño variability in the equatorial Tropical Pacific is characterized by sea-surface temperature anomalies and associated changes in the atmospheric circulation. Through an enormous monitoring effort over the last decades, the relevant time scales and spatial patterns are fairly well-documented. Anna von der Heydt and Henk Dijkstra describe the hierarchy of models that have been developed to understand the physics of this phenomenon and to make predictions of future variability. It turns out that the predictability of El Niño events is still limited to about 6–9 months due to inherent nonlinear processes.

About once every four years, the sea surface temperature in the equatorial eastern Pacific is a few degrees higher than normal [13]. Near the South American coast, this warming of the ocean water is usually at its maximum around Christmas. Long ago, Peruvian fishermen called it El Niño, the Spanish phrase for the 'Christ Child'. During the last decades, the equatorial Pacific has been observed in unprecedented detail [10]. The El Niño relevant quantities in the equatorial ocean and atmosphere system are sea-level pressure, sea-surface temperature, sea-level height, surface wind and ocean sub-surface temperature.

What makes El Niño unique among other interesting phenomena of natural climate variability is that it has both a well-defined pattern in space and a relatively well-defined time scale. The sea-surface temperature anomaly during the maximum of the El Niño 1997–1998, in December 1997, obtained by subtracting a long term mean (see Figure 1a) from the actual pattern, is shown in Figure 1b. The anomaly is characterized by higher than usual equatorial Pacific temperatures east of the date line [14]. A scalar index of this sea-surface temperature anomaly pattern is the NINO3 index, defined as the sea-surface temperature anomaly averaged over the region $5°$S–$5°$N, $150°$W–$90°$W (see the black box in Figure 1a). In the time series (Figure 1c), the high NINO3 periods are known as El Niño's and the low NINO3 periods as La Niña's. Most El Niño's and La Niña's peak around December and are hence phase-locked to the seasonal cycle.

The mean surface winds over the equatorial Pacific, the trade winds, blow from east to west and are driven by an area of average high pressure in the eastern part of the Pacific and a low pressure area over Indonesia. The Southern Oscillation consists of an irregular strengthening and weakening of the trade winds, related to the changes in surface pres-

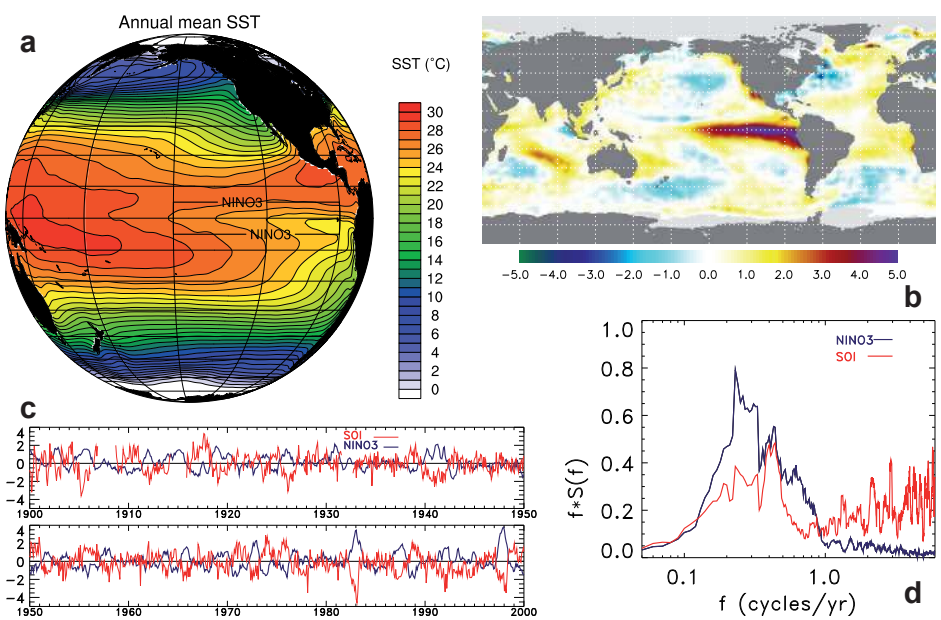

Figure 1 (a) The time mean sea-surface temperature of the Pacific Ocean. The black box indicates the NINO3 region. (b) Sea-surface temperature anomaly field of December 1997, at the height of the 1997/1998 El Niño. (c) Monthly mean SOI and NINO3 index over the period 1900–1999. (d) Spectra of monthly mean SOI and NINO3. Shown are normalized periodograms smoothed over 11 bins, that is over 0.11 cycles per year. Note that the x-axis is logarithmic, and $f \times S(f)$ rather than $S(f)$ is shown, in order that equal areas make equal contributions to the variance.

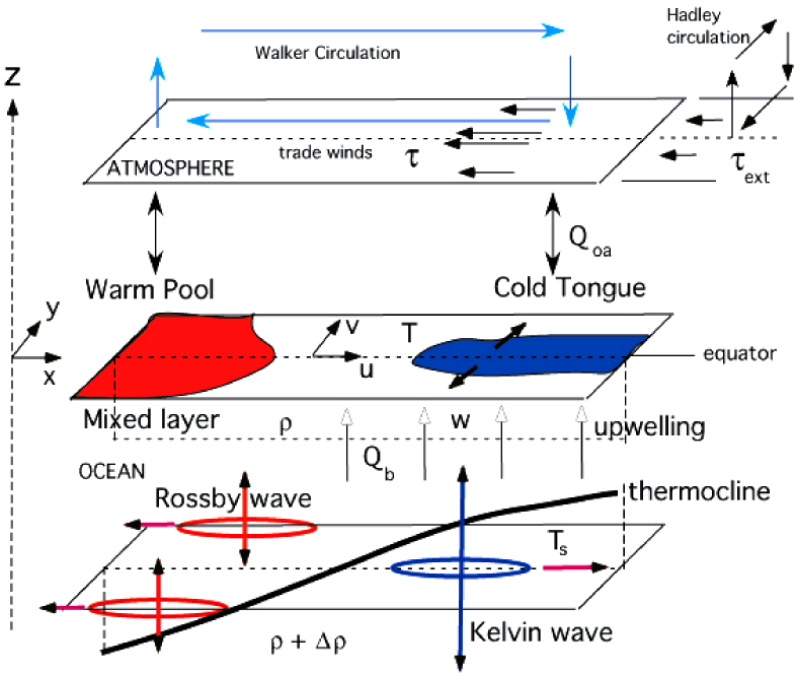

Figure 2 Overview of the oceanic and atmospheric processes of the equatorial coupled ocean-atmosphere system.

sure. An index that captures the amplitude of the sea-level pressure anomaly pattern is the Southern Oscillation Index (SOI), which is the normalized difference of the pressure anomalies between Tahiti (18°S, 150°W) and Darwin (12°S, 131°E).

It was Jacob Bjerknes [1] who discovered that El Niño and the Southern Oscillation are part of the same phenomenon now referred to as ENSO. Generally, periods with a high NINO3 index have a low SOI and vice versa (Figure 1c) which indicates that the trade winds are weaker (stronger) during El Niño's (La Niña's). The average time scale of ENSO is about four years, as can be seen from the spectra of the NINO3 index and the SOI in Figure 1d. The SOI contains more high-frequency variability than the NINO3 index.

Basic processes

The vertical structure of the upper ocean can be considered as layered with a well-mixed upper layer down to a depth of 50 m and a sharp transition between warm and cold water (the thermocline) at about 150 m depth (Figure 2). The temperature in the mixed layer changes due to air-sea interaction, exchange processes with deeper layers and advection. Let the net heat flux from the atmosphere into the ocean and that at the bottom of the mixed layer be denoted by Q_{oa} and Q_b (positive when heat is going into the mixed layer), respectively. Under the approximation that the temperature is vertically homogeneous over the layer, one can integrate the heat balance equation over the layer which results in an equation for the mixed-layer temperature T, i.e.

$$\frac{\partial T}{\partial t} = -(u\frac{\partial T}{\partial x} + v\frac{\partial T}{\partial y}) + F_T^H + \frac{Q_{oa} + Q_b}{\rho C_p H_m}, \quad (1)$$

where C_p is the heat capacity of water, H_m the mean depth of the mixed layer, ρ its mean density and where (u, v) are the horizontal velocities in the mixed layer. The quantity F_T^H represents the horizontal mixing of heat through lateral turbulent exchange processes. Equation (1) expresses that the mixed layer temperature can change due to advection (first two terms in the right hand side), horizontal exchange (third term) and vertical exchange (last term) of heat.

The effects of the wind stress on the upper ocean are threefold. The wind stress due to the trade winds causes water to pile up near the western part of the basin. This induces a higher pressure in the upper layer western Pacific than that in the eastern Pacific and consequently a shallowing of the thermocline towards the east (Figure 2). Second, these winds cause a divergence of mass at the equator that is compensated by vertical mass transport, the so-called upwelling. Finally, the wind stress is responsible for the presence of the upper ocean currents.

When the amplitude and/or the direction of the wind stress changes, the upper ocean adjusts through wave dynamics. The most important waves involved in this adjustment process are:

1. Equatorial Kelvin waves. For such a wave, the meridional structure of the thermocline is maximal at the equator. Its amplitude decays exponentially in meridional direction with a decay scale λ_0 of about 300 km. The zonal velocity has the same spatial structure as the thermocline and the meridional velocity is zero. The group velocity of these non-dispersive waves, say c_o, is about 2 ms^{-1}. It takes about $\tau_K = 3$ months for the wave to cross the Pacific basin of width $L = 15{,}000$ km.
2. Long equatorial Rossby waves. For such a wave, the meridional thermocline structure has an off-equatorial maximum. For each of these waves, the meridional velocity is much smaller than the zonal velocity. The group velocity of these non-dispersive waves is $c_j = -c_o/(2j+1)$. The $j = 1$ long Rossby wave travels westward with a velocity which is 1/3 of that of the Kelvin wave and hence takes about $\tau_R = 9$ months to cross the Pacific basin.

When a Kelvin wave meets the east coast, the dominant contribution of the reflected signal are long Rossby waves. Similarly, when a Rossby wave meets the west coast, it is reflected dominantly as a Kelvin wave.

The coupling of the ocean-atmosphere system can be understood by looking at the effect of sea-surface temperature anomalies. A sea-surface temperature anomaly will give through local heating (as measured by a parameter α_T) a lower-level wind stress anomaly (as measured by a parameter γ). The resulting wind stress anomaly on the ocean-atmosphere surface will: (i) change the thermocline slope through horizontal pressure differences in the upper ocean; (ii) change the strength of the upper ocean upwelling; and (iii) affect the upper ocean currents (u, v) in the mixed layer. The changes in velocity field and thermocline field will affect the sea surface temperature, according to (1).

The strength of the coupling in the system, i.e. between the atmosphere and the ocean, is determined by the combined effects of how much zonal wind anomaly is generated by sea-surface temperature anomalies and how much of the momentum of this wind is transferred as stress to the upper ocean layer. The strength of the coupling is measured by the parameter μ which is a (dimensionless) product [3] of α_T and γ, i.e.

$$\mu = \frac{\gamma \alpha_T \Delta T L^2}{c_o^2 c_a^2}, \quad (2)$$

where the quantity ΔT is the mean zonal temperature difference over the basin, L the zonal length of the basin and $c_a = 60\ \mathrm{m}s^{-1}$ the free Kelvin wave speed in the atmosphere.

Physics of El Niño variability

Much of the theory on El Niño variability was developed with the help of the Zebiak–Cane (ZC) model [19], which precisely represents the physical processes in Figure 2. In this model the zonal wind stress τ^x over the ocean is represented by

$$\tau^x = \tau^x_{ext} + \mu A(T), \qquad (3)$$

where $A(T)$ represents the atmospheric response of the model to the sea-surface temperature T. The part τ^x_{ext} is determined externally, i.e, by processes outside the Pacific basin and it is usually taken to be constant.

At zero coupling strength ($\mu = 0$), the ocean circulation and consequently the sea-surface temperature is determined by the external zonal wind stress τ^x_{ext}. A small easterly wind causes a small amount of upwelling and a small slope in the thermocline. At small μ, additional easterly wind stress due to coupling occurs because of the zonal temperature gradient. This leads to larger upwelling and a larger thermocline slope, strengthening the cold tongue in the eastern part of the basin.

With increasing μ, the Pacific climate state becomes unstable. Necessary conditions for instability can be obtained by determining the linear stability boundary through normal mode analysis. In such an analysis, an arbitrary perturbation is decomposed in modes (e.g. Fourier modes) and the growth or decay of each of these modes is investigated. When the background state is stationary, the time-dependence of each mode is of the form $e^{\sigma t}$, where $\sigma = \sigma_r + i\sigma_i$ is the complex growth rate. If μ is the control parameter, then the linear stability boundary μ_c is the first value of μ where $\sigma_r = 0$ for one particular normal mode. A mode with $\sigma_i \neq 0$ is oscillatory (with a period $2\pi/\sigma_i$) while a mode with $\sigma_i = 0$ is called stationary. If the growth factor of a mode is positive, sustained oscillations will occur and if it is negative the mode will be damped. In the presence of atmospheric noise, however, the spatial pattern of a damped mode can still be excited. [4] provides an overview of the dependence of the growth factor (Figure 3a) and period (Figure 3b) of the least stable mode (the ENSO mode) on the background conditions. The dashed curves in Figure 3 represent zero growth (so-called neutral conditions) of the ENSO mode. Present-day estimates for the Pacific background state correspond to the area near the points A and B, with a period of 2–6 years and near neutral conditions.

The main positive feedbacks responsible for the instability of the coupled ocean-atmosphere system are referred to the thermocline, upwelling and zonal advection feedback [12]. The thermocline feedback can be described as follows. A positive sea-surface temperature anomaly in the eastern Pacific will lead to a weakening of the trade winds to the west of this anomaly. This will lead to a smaller slope of the thermocline and hence the cold water will be further away from the surface in the east. This causes a positive heat flux Q_b in (1) which will amplify the initial disturbance. The upwelling feedback can be understood in a similar way, considering again a positive sea-surface temperature anomaly in the eastern part of the basin and associated changes in the wind. In this case, weaker easterly winds induce less upwelling and hence less cold water enters the mixed layer, again amplifying the sea surface temperature perturbation. The zonal advection feedback arises through zonal advection of heat, particularly in regions of strong sea surface temperature gradients. A warm sea-surface temperature anomaly then can lead to wind anomalies, and, if positive, intensify zonal ocean currents, which bring more warm water to the location of the original perturbation.

In the ZC model, oscillatory El Niño behaviour is found slightly above critical conditions. Attempts have been made to derive conceptual models to explain the physics of the oscillation period. Most of these share the ideas that one of the positive feedbacks acts to amplify sea-surface temperature anomalies and that wave adjustment processes in the ocean eventually cause a delayed negative feedback. These common elements are grouped together in the delayed oscillator mechanism. The differences between the views are subtle [6] and are related to the role of the boundary wave reflections, the dominant feedback which is responsible for amplification of anomalies and the view of the dynamical adjustment processes in the ocean. There are four types of ENSO 'oscillators': (i) the 'classical' delayed oscillator; (ii) the recharge/discharge oscillator; (iii) the western Pacific oscillator; and (iv) the advective/reflective oscillator. Below, we only describe (i), the other oscillators are described extensively in [6] and [18].

In the 'classical' delayed oscillator view, the eastern boundary reflection is unimportant, the thermocline feedback is dominant and individual Kelvin and Rossby waves control ocean adjustment. A minimal model [15]

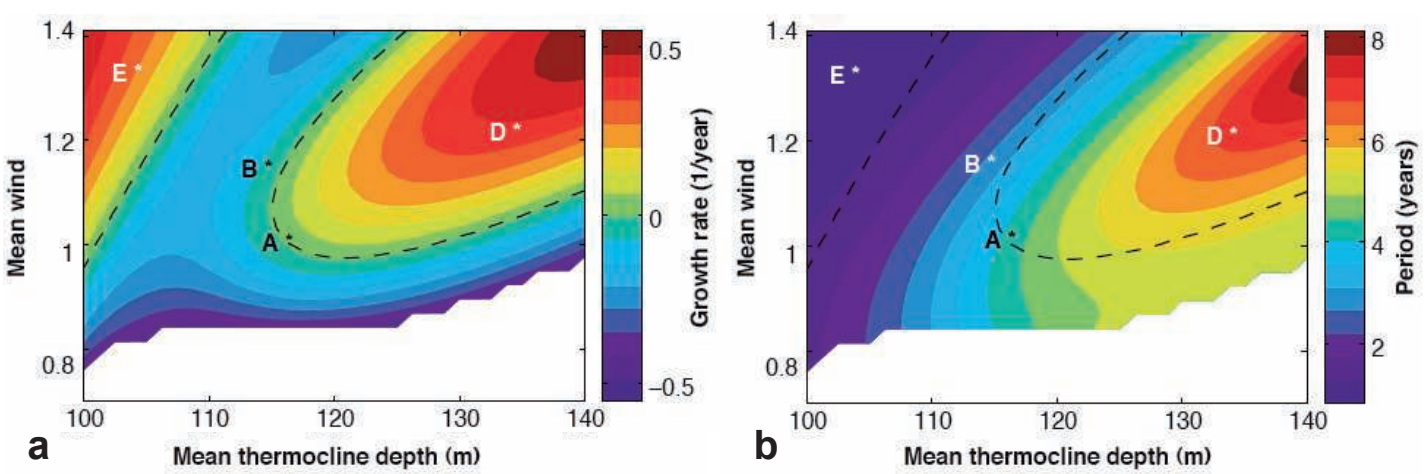

Figure 3 Dependence of (a) growth rate (σ_r in yr^{-1}) and (b) period ($2\pi/\sigma_i$ in yr) of the ENSO mode on the mean wind intensity (in units of 0.5 $\mathrm{cm}^2\mathrm{s}^{-2}$) and the mean thermocline depth (in m) [4].

representing this behaviour is a differential delay equation of the form

$$\frac{dT(t)}{dt} = ah_e(x_c, t-\tau_1) - bh_o(x_c, t-\tau_2) - cT^3(t). \quad (4)$$

In this equation, a, b and c are constants, T is the eastern Pacific temperature anomaly, which is influenced by midbasin (at $x = x_c$) equatorial thermocline depth anomalies h_e and off-equatorial anomalies h_o. Furthermore, $\tau_1 = \frac{\tau_K}{2}$ and $\tau_2 = \frac{\tau_R}{2} + \tau_K$ where τ_K and τ_R are the basin crossing times of the Kelvin wave and the gravest ($j = 1$) Rossby wave.

When a Kelvin wave, which deepens the thermocline, arrives in the eastern Pacific, local amplification of temperature perturbations occurs through the thermocline feedback, represented by the first term in the right hand side of (4). The wind response excites (off-equatorial) Rossby waves which travel westwards, reflect at the western boundary and return as a Kelvin wave which rises the thermocline and provides a delayed negative feedback (second term in (4)). The delay τ_2 is the time taken for the Rossby wave to travel from the centre of wind response to the western boundary plus the time it takes the reflected Kelvin wave to cross the basin. The nonlinear in (4) term is needed for equilibration to finite amplitude.

A linear mechanism for ENSO's phase locking to the seasonal cycle was proposed in [5]. The coupling strength μ varies on a seasonal time scale and is maximal during June–July and minimal during December–January. The variation of the eastern Pacific thermocline depth h in the 'classical' delayed oscillator picture can be described by

$$\frac{dh(t)}{dt} = dF(\mu(t-\tau_1)h(x_c, t-\tau_1)) - eF(\mu(t-\tau_2)h(x_c, t-\tau_2)) - fh(t). \quad (5)$$

Here F is a certain nonlinear function, the damping of thermocline anomalies is assumed to be linear (the third term in the right hand side of (5)) and d, e and f are again constants. At peak time of ENSO, the eastern thermocline anomalies are maximal and hence $dh/dt \approx 0$. For small dissipation, the warming by the Kelvin wave (first term in (5)) has to balance the cooling due to the Rossby wave (second term in (5)).

Suppose that the peak of ENSO would occur during June, i.e. with maximum μ. In this case, the warm Kelvin wave was excited during April and because coupling is strong over April–June, it has a relatively large amplitude. The Rossby wave was, however, excited about 6 months earlier, i.e. during November–December when coupling was small. It has therefore a small amplitude and cannot balance that of the Kelvin wave ($\mu(t-\tau_1)h(x_c, t-\tau_1)$ is large while $\mu(t-\tau_2)h(x_c, t-\tau_2)$ is small). On the other hand, when peak conditions are in December, the Kelvin wave is excited in October during relatively small coupling and its amplitude is only weakly amplified. The Rossby wave is now excited in June when coupling is large and is amplified to significant amplitude to balance the Kelvin wave thermocline signal.

ENSO's predictability barrier

Two different mechanisms have been suggested to explain the irregularity of ENSO, as for example seen in the NINO3 time series (Figure 1c). These are: (i) deterministic chaotic behaviour; and (ii) impact of small-scale processes usually referred to as 'noise', possibly through non-normal growth behaviour.

Deterministic chaotic behaviour can result from nonlinear resonances due to interaction of the seasonal cycle and the ENSO mode [7, 16], leading to frequency locking. A typical example of a one-dimensional map where frequency locking occurs is the circle map given by

$$x_{n+1} = x_n + \Omega - \frac{K}{2\pi}\sin 2\pi x_n \pmod 1 \quad (6)$$

on the interval $[0, 1)$. Here, mod 1 indicates that if x_n becomes larger than 1 or smaller than 0, its value is adjusted by adding or subtracting 1 to get a value within the unit interval. $\Omega \in [0, 1)$ can be considered to be the forcing frequency and the control parameter K is a measure of the nonlinearity of the system. To look for frequency locked regions, one varies Ω for fixed K and searches for rational rotation numbers W defined by

$$W = \lim_{n\to\infty} \frac{x_n - x_0}{n}, \quad (7)$$

where in this definition the value of x_n is considered, without the mod 1 function.

When the coupling strength μ is increased above criticality in the seasonally forced ZC model the NINO3 index displays regimes of frequency locking to the annual cycle alternated by chaotic regimes [8]. In these frequency-locked regimes, the ENSO period is a rational multiple of the seasonal cycle. When δ_s indicates the parameter which measures the strength of the upwelling feedback, the behaviour of the ZC model in the (μ, δ_s) parameter plane is captured [8] in the so-called Devil's terrace (Figure 4). The colours indicate the frequency ratio of frequency locked solutions and the grey areas indicate the chaotic solutions. Although chaotic solutions are nearly everywhere in parameter space over a fractal surface, the locked regime is broad, with the frequency ratio becoming smaller for smaller δ_s. For many solutions found, the phase lock-

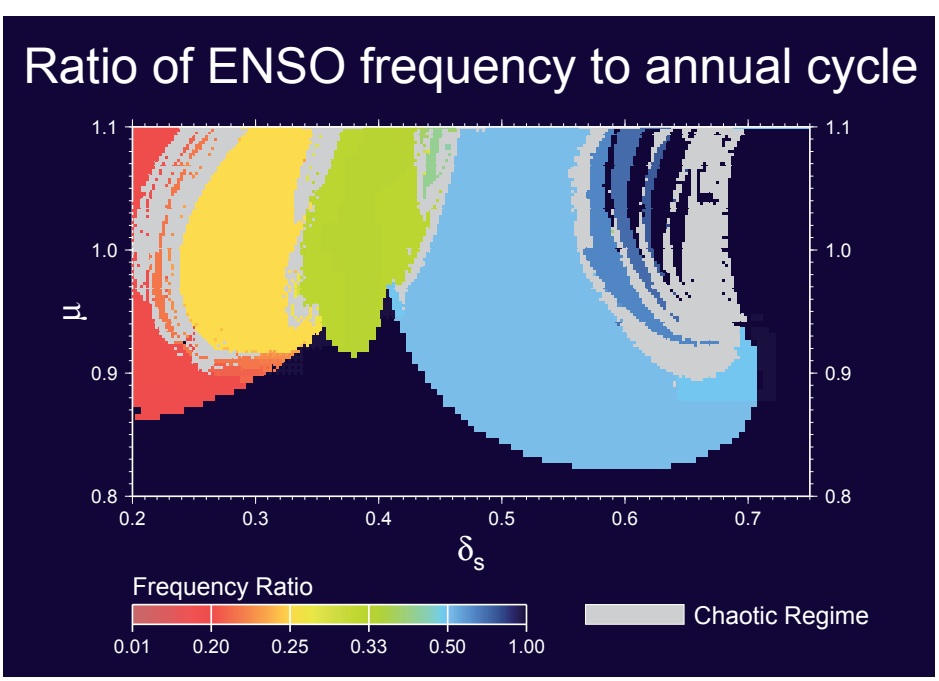

Figure 4 The Devil's terrace as computed in [8]. Colours indicate the frequency locked regimes, with chaotic regimes in between. Along a section for fixed μ, a so-called Devil's staircase appears.

ing to the annual cycle is near to that observed with January being the preferred month of the peak of the warm event.

From the perspective of El Niño, processes that evolve independently with smaller time and space scales can be considered as noise. In the atmosphere, for example, the 30–60 day or Madden–Julian oscillation [9] gives rise to westerly wind bursts. These are events of anomalous westerlies lasting typically a week, which are strongest somewhat west of the region of the El Niño wind response. Kelvin waves are excited very effectively by the Madden–Julian oscillation because they travel eastward with a similar speed. The spectra of the NINO3 index and the SOI in Figure 1 are moderately peaked compared to those of many deterministic versions of the ZC model. Hence, it is generally agreed that noise contributes substantially to the irregularity of El Niño. If the Tropical Pacific climate system is close to neutral conditions, non-normal growth of perturbations, which occurs because the operator in the ZC model is not self-adjoint, can lead to additional irregular behaviour [11].

During boreal spring the coupled ocean-atmosphere system is thought to be at its frailest state. Then the system is most susceptible to perturbations, which can be internal small-scale stochastic events (random wind bursts) or random external influences (like the monsoon). This leads to a spring predictability barrier in April/May independent of when the forecast is started. The existence of this barrier (still) limits the predictability of El Niño (with a broad range of models) to about 6–9 months.

Another issue is to predict how the characteristics of ENSO variability, such as amplitude or frequency change under global warming. In this case, the pattern of the long-term mean climate in the tropical Pacific becomes a crucial factor, because this pattern partly determines the strength of the different feedbacks involved. It is still not clear whether the ENSO system is above criticality or just below criticality (and hence excited by noise). Future changes in the global climate as a whole can therefore have a significant impact on the characteristics of ENSO variability. When it comes to predictions of long-term changes in ENSO characteristics under global warming, state-of-the-art climate models project a wide range of changes to future ENSO variability [2], indicating that the interaction of the long-term mean state of climate and modes of inter-annual variability remains poorly understood. A study with a ZC type model has indicated that changes in the background temperature and external wind stress mainly shift the position of the cold tongue in the eastern equatorial Pacific [17]. Such a shift affects local temperature gradients and can impact the relative strength of the different feedbacks, e.g. strengthen the zonal advection feedback. From the perspective of Figure 3, a change in the background climate could move the ENSO system across the critical stability threshold (dashed curve in Figure 3).

Summary

Although there are still many issues which are not sufficiently well explored, we can conclude that the ENSO phenomenon can be understood within a (weakly) nonlinear framework of equatorial ocean-atmosphere interaction. The oscillatory nature of ENSO derives from an internal mode of variability of the coupled system involving coupled feedbacks and (ocean) wave dynamics. Possible mechanisms for ENSO irregularity have been suggested, but it is not clear at the moment which one is dominant. Noise and the inherent instability of the system are important limiting factors for the predictability of El Niño. The growth of perturbations depends on the season and leads to a spring predictability barrier.

References

1 J.P. Bjerknes, Atmospheric teleconnections from the equatorial Pacific, *Monthly Weather Review* 97 (1969), 163–172.

2 M. Collins, The El Niño - Southern Oscillation in the second Hadley Centre Coupled model and its response to greenhouse warming, *Clim. Dyn.* 24 (2005), 89–104.

3 H.A. Dijkstra, *Nonlinear Physical Oceanography: A Dynamical Systems Approach to the Large Scale Ocean Circulation and El Niño*, Springer, New York, 2005.

4 A. Fedorov and S. Philander, Is El Niño Changing?, *Science* 288 (2000), 1997–2002.

5 E. Galanti and E. Tziperman, ENSO's phase locking to the seasonal cycle in the fast-SST, fast-wave and mixed-mode regimes, *J. Atmos. Sci.* 57 (2000), 2936–2950.

6 F.-F. Jin, An equatorial recharge paradigm for ENSO. II: A stripped-down coupled model, *J. Atmos. Sci.* 54 (1997), 830–8847.

7 F.-F. Jin, J.D. Neelin and M. Ghil, El Niño on the devil's staircase: Annual subharmonic steps to chaos, *Science* 264 (1994), 70–72.

8 F.-F. Jin, J.D. Neelin and M. Ghil, El Niño/Southern Oscillation and the annual cycle: Subharmonic frequency-locking and aperiodicity, *Physica D* 98 (1996), 442–465.

9 R. Madden and P. Julian, Observations of the 40-50-day tropical oscillation — A review, *Monthly Weather Review* 122 (1994), 814–835.

10 M. McPhaden and co-authors, The Tropical Ocean-Global Atmosphere observing system: a decade of progress, *J. Geophys. Res.* 103 (1998), 14,169–14,240.

11 A.M. Moore and R. Kleeman, Stochastic Forcing of ENSO by the Intraseasonal Oscillation, *J. Climate* 12 (1999), 1199–1220.

12 J.D. Neelin, The slow sea surface temperature mode and the fast-wave limit: Analytic theory for tropical interannual oscillations and experiments in a hybrid coupled model, *J. Atmos. Sci.* 48 (1991), 584–606.

13 S.G.H. Philander, *El Niño and the Southern Oscillation* Academic Press, New York, 1990.

14 E. Rasmusson and T.H. Carpenter, Variations in tropical sea surface temperature and surface wind fields associated with the Southern Oscillation/El Niño, *Monthly Weather Review* 110 (1982), 354–384.

15 M. Suarez and P.S. Schopf, A delayed action oscillator for ENSO, *J. Atmos. Sci.* 45 (1988), 3283–3287.

16 E. Tziperman, L. Stone, M.A. Cane and H. Jarosh, El Niño chaos: overlapping of resonances between the seasonal cycle and the Pacific ocean-atmosphere oscillator, *Science* 264 (1994), 72–74.

17 A.S. von der Heydt, A. Nnafie and H.A. Dijkstra, Cold tongue/Warm pool and ENSO dynamics in the Pliocene, *Clim. Past* 7 (2011), 903–915.

18 C. Wang and J. Picaut, Understanding ENSO physics: A review, In C. Wang, S.-P. Xie, and J.A. Carton, editors, *Earth's Climate: The Ocean-Atmosphere Interaction*, pages 21–48. American Geophysical Union.

19 S.E. Zebiak and M.A. Cane, A model El Niño-Southern Oscillation, *Monthly Weather Review* 115 (1987), 2262–2278.